Journal of Interfaces, Thin films, and Low dimensional systems 8 (1) Summer and Autumn (2024) 803-810

The characteristics of nickel-based elliptical cylinder plasmonic nano-waveguides in the near-infrared wavelength

Scientific research paper

M. R. Jafari[1*], M. Ghanaati[1], A. Asadi[2]

[1]*Department of Condensed Matter, Faculty of Physics, Alzahra University, Tehran, Iran*

[2]*Department of Physics, Faculty of Science, Imam khomeini University of Maritime Science, Nowshahr, Iran*

ARTICLE INFO

Article history:
Received 27 July 2024
Revised 12 September 2024
Accepted 19 September 2024
Available online 19 December 2024

Keywords
Nickel
Nano-Waveguide
Plasmonic
Finite Element Method

ABSTRACT

In this article, a nickel-based elliptical cylinder plasmonic nano-waveguide (NECPNW) layer is used to serve the coating purpose. The results of this purposed structure that are yielded by the finite element method in the COMSOL-multi-physics simulator program reflect that this approach has the capacity for more field confinement and simultaneously less dissipation. As a result, surface plasmons (SPs) can be utilized to improve data exchange. Our results have displayed that the proposed waveguide has a figure of merit over 35000, propagation length over 470 µm, and a normalized mode area of $\sim 10^{-3}$ by tuning the semi-major axis Ni nanowire, wavelength of incident light, and the thickness of the dielectric layers. Hence, the proposed waveguide shows longer propagation length and better figure of merit than the similar plasmonic waveguides.

1 Introduction

The extraordinary advantages of surface plasmons (SPs) in compressing light into regions much smaller than the diffraction limit, have made them conceivable candidates for the manufacture and confinement of optical coordinate circuit components [1-5]. In some previous waveguides, noble metals [6] have been properly utilized for SPs [7] modes, including nanowires [8-13], wedge waveguides [14], waveguides with dielectric charge [15], and etc. Nevertheless, they are still involved with some problems such as field limits. To solve this problem, the hybrid plasmonic waveguides (HPWs) [16-32] have been utilized instead of waveguides based on noble metals [33-35], with the hope that they would result in less dissipation and more field confinement. However, in practice, the desired results have not been obtained, so it is still of vital importance for researchers to achieve desired results in plasmonics. In several studies that we will refer to in the following, the characteristics of the sodium metal have been examined for their applications in plasmonic waveguides. In a plasmonic nanolaser based on sodium metal, Yang and colleagues [36] found that sodium has incorporated a lower diffraction limit at near-infrared wavelengths. In another study, Tao and his colleagues [37,38] pinpointed the existence of directional sets in plasmonic waveguides based on sodium metal, and Da Teng and his colleagues [39] proposed two sodium nanowires based on sodium metal with two layers of dielectric coating. Comparing them with silver metal, Da Teng and his colleagues observed that the nanowire Na shows less dissipation and more grounded field confinement. Recently a palladium-based elliptical cylinder plasmonic waveguide (PECPW) with two dielectric layers as a coating in different states has been taken under consideration [40]. They showed that the highest value for the propagation length L_{spp} and the

*Corresponding author.
Email address: Mo.jafari@Alzahra.ac.ir
DOI: 10.22051/jitl.2024.47006.1108

figure of merit FOM of this waveguide is for a case of single palladium nanowire with *b=4a* and without any dielectrics. In this paper, we propose a plasmonic nanowaveguide based on nickel metal within the near infrared range (NIR) run in which longer propagation distances exist, where better figure of merit (FOM) and stronger confinement are expected in comparison to the similar plasmonic waveguides (e.g., see [40, 41]). In this paper, the characteristics of the suggested nanowaveguide have been examined based on the finite element method and in accordance with the wavelength and various thicknesses of the dielectric layers. The results demonstrate that a cylinder elliptical plasmonic waveguide based on nickel metal has a longer propagation length, lower dissipation and smaller ordinary mode region compared to sodium metal. However, the results are not as promising as those of PECPW. As a result, nickel metal can be utilized in nanophotonic circuits.

2 Waveguide design and mathematical formulation

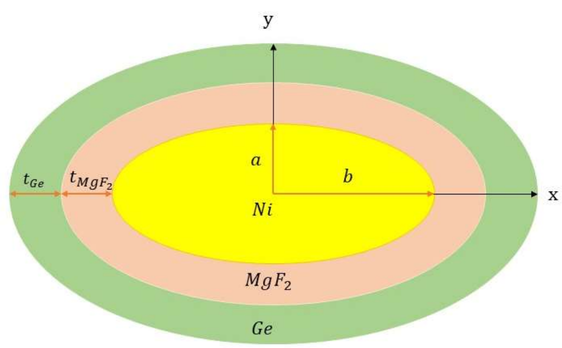

Figure 1. The cross-section of the proposed NECPNW.

Figure 1, shows the cross-section of the plasmonic waveguide structure based on nickel metal. In this structure an elliptical cylinder nanowire with two dielectric layers (MgF_2 and Ge) is used. As you can see, a and b are respectively, the semi-minor axis and semi-major axis of the proposed waveguide cross section. t_{MgF_2} is the thickness of the MgF_2 dielectric layer with a relative permittivity of $\varepsilon_{MgF_2} = 1.7$ [39] and t_{Ge} is the thickness of the Ge dielectric layer with a relative permittivity of $\varepsilon_{Ge} = 16.2$ [39]. Investigation and analysis of surface plasmon polaritons propagation mode in NECPNW structure is done in very small dimensions for wavelength $400 - 1000$ nm. In addition, it is possible to calculate the dielectric function of nickel metal using the Drude-Lorentz modal, which is expressed as [41]:

$$\varepsilon_{DL}(\omega) = \varepsilon_1 + i\varepsilon_2 = \varepsilon_b - \frac{\omega_p^2}{\omega^2 + i\omega\gamma_p} + \frac{f_1\omega_1^2}{\omega_1^2 - \omega^2 - i\omega\gamma_1}. \tag{1}$$

The parameters used in calculating the dielectric function of nickel are according to Table 1, [42]:

Table 1. Drude-Lorentz model coefficients used for nickel [42].

Parameter	Value
f_1	0.137
ω_1	0.415 eV
γ_1	0.765 eV
ω_p	13.28 eV
γ_p	0.038 eV

The effective refractive index of the proposed waveguide is calculated as [40]:

$$n_{\text{eff}} = \frac{k_z}{k_0}, \tag{2}$$

where k_0 is the wave number in vacuum and k_z is the component of z the wave number. The complex effective mode index is solved as [7]:

$$n_{\text{eff}} = n_{\text{eff-r}} + in_{\text{eff-i}}, \tag{3}$$

In addition, the propagation length is obtained from equation (4), [40]

$$L_{spp} = \frac{1}{k_0 \text{Im}(n_{\text{eff}})}, \tag{4}$$

A_{n}, A_{eff} and A_0 respectively, represent the normalized mode area, the effective mode area, and the diffraction limited mode region in the vacuum environment, and their relationship is as [40]:

$$A_{\text{n}} = \frac{A_{\text{eff}}}{A_0} = \frac{1}{A_0} \frac{\int_{-\infty}^{+\infty} W(x,y)dx\,dy}{\max[W(x,y)]}, \tag{5}$$

So that, W(x,y) is the energy density of waveguide plasmon mode [40] and is defined as:

$$W(x,y) = \frac{1}{2} Re\left\{\frac{d[\varepsilon_0 \varepsilon_r(x,y)\omega]}{d\omega}\right\} |E(x,y)|^2 + \frac{1}{2}\mu_0 |H(x,y)|^2 . \quad (6)$$

Finally, the waveguide figure of merit criterion is [43] calculated by:

$$FOM = \frac{L_{\mathrm{SPP}}}{\sqrt{\frac{A_{\mathrm{eff}}}{\pi}}} . \quad (7)$$

The Results of this research have been obtained using the finite element method in the COMSOL-Multiphysics 6.0 software based on the mentioned parameters and variables.

3 Results and discussion

Figure 2, shows how the electric field is confined in the NECPNW structure when no dielectric is used where $a = 50$ nm and different values of *b=a, 2a, 4a* are predicted for the main radius and wavelength of $\lambda = 400 - 1000$ nm. As can be seen in Fig. 2(a), in the case where b=a, a relatively strong electric field is created around the surface of the nickel metal, and with increasing the value of b, that is, for Figs. 2(b) and 2(c) in which the semi-major axis of $b = 100$ nm and $b = 200$ nm are considered respectively, the electric field is created on both sides of *b* and this quantity increases with the increase of *b*. Figure 2(d) shows that the diagram of the electric field around the nanowaveguide is drawn in the direction of the y axis according to the mentioned structure.

Figure 3 illustrates the results of the propagation of the plasmonic nanowaveguide based on nickel metal in the case where no dielectric is used. In this structure $t_{\mathrm{MgF_2}} = t_{\mathrm{Ge}} = 0$ and the semi-minor axis of the nanowire section $a = 50$ nm and three different values the semi-major axis of the nanowire section $b = 50, 100, 200$ nm are considered. In Fig. 3(a) it can be seen that the real part of effective mode index decreases with the increase of λ and *b*. Figure 3(b) shows that the propagation length has increased with the increase of wavelength and the semi-major axis, and this nanowaveguide has resulted in a longer propagation length compared to the waveguide based on sodium metal. Figure 3(c) shows that the normalized mode area for a given quantity of A_{n} of the nanowire for the semi-major decreases with the increase of the wavelength and for different values of the semi-major axis at a given wavelength it also increases with the increase of *b*. Figure 3(d) shows the changes of the nanowire figure of merit in terms of wavelength, which increases with the increase of the wavelength and the size of the semi-major axis.

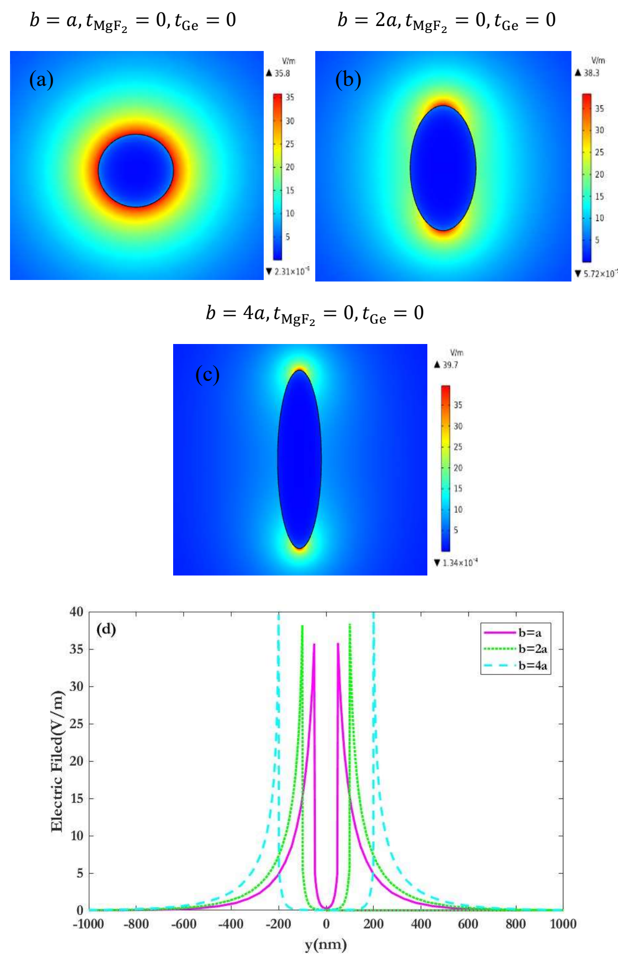

Figure 2. Distribution of the electric field in the cross-section of the elliptical cylinder nanowire at (a) *b=a*, (b) *b=2a*, (c) *b=4a*, and (d) the electric field distribution in y-direction.

Figure 4 shows the distribution of the electric field around the nickel nanowire for the elliptical cylinder nanowave with MgF_2 dielectric coating for $a = 50$ nm and $b = 4a$ and different values of $t_{\mathrm{MgF_2}}$. As can be seen in Figs. 4(a), 4(b), and 4(c), the thickness of the dielectric coating is considered to be 10, 15, and 20 nm, respectively, and the intensity of the modal field on both

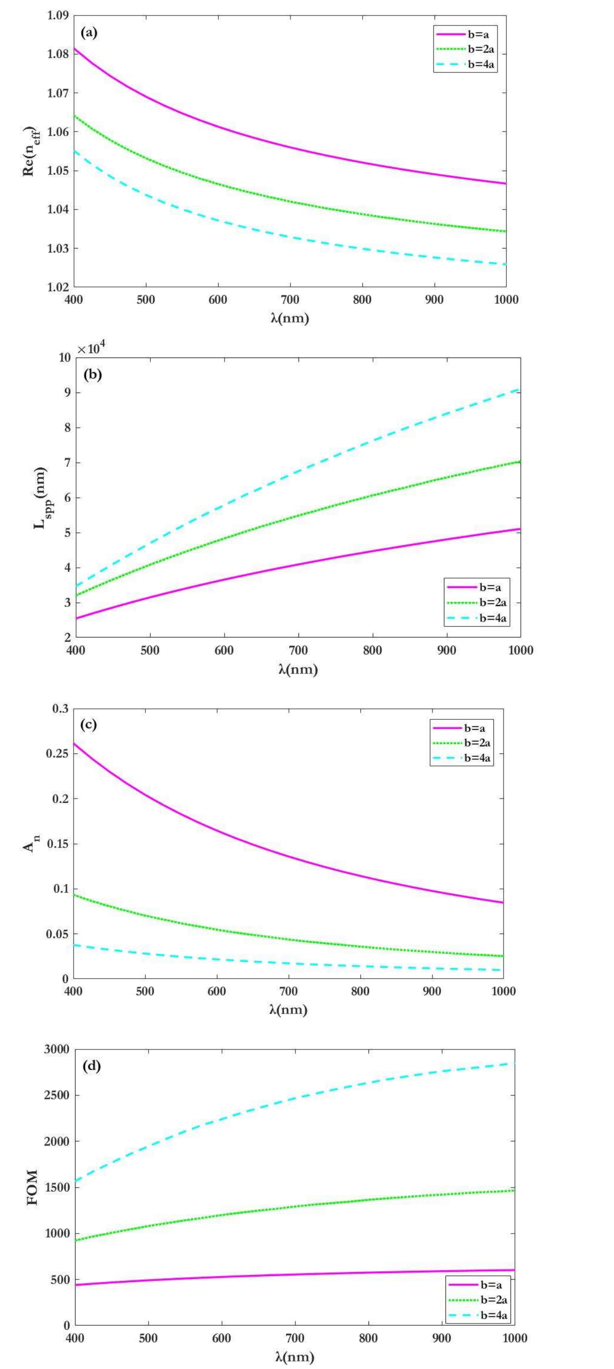

Figure 3. Modal properties nanowire in vacuum without dielectric coating for different values of semi-major axis. (a) $\mathrm{Re}(n_{\mathrm{eff}})$, (b) L_{spp}, (c) A_{n} and (d) FOM.

sides of the semi-major axis of the nanowire decreases with the increase of the dielectric thickness. In Fig. 4(d), the diagram of the modal field around the nanowaveguide for the above values is drawn in the direction of the y axis.

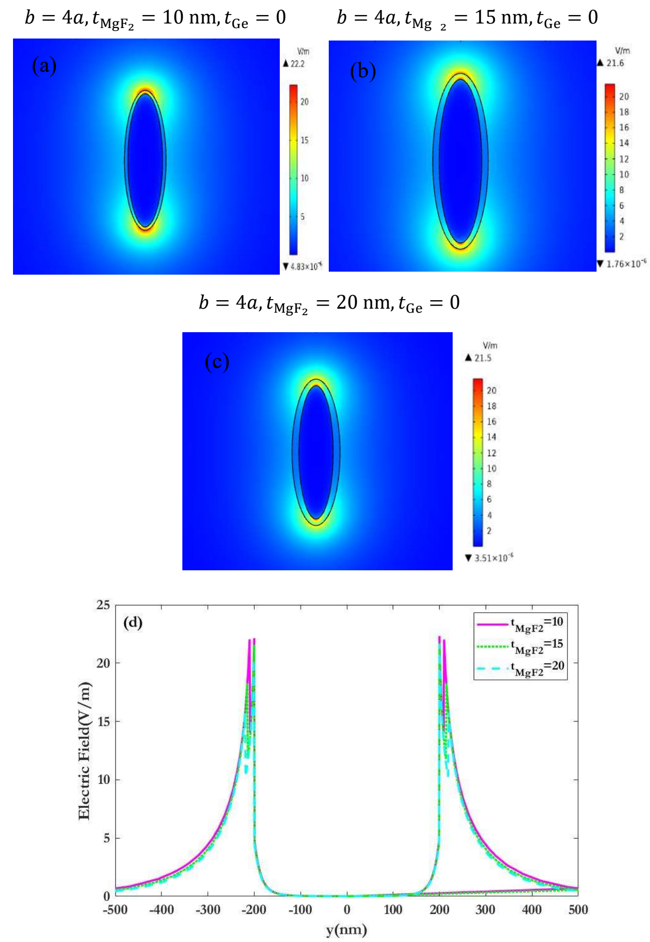

Figure 4. Distribution of the electric field in the cross-section of NECPNW with dielectric coating $\mathrm{MgF_2}$ and *b=4a*. (a) $t_{\mathrm{MgF_2}} =$ 10 nm, (b) $t_{\mathrm{MgF_2}} = 15$ nm, (c) $t_{\mathrm{MgF_2}} = 20$ nm and (d) distribution of the electric field in the cross-section of NECPNW for different values of the $t_{\mathrm{Mg}\;2}$.

The different parts of Fig. 5 show the behavior of $\mathrm{Re}(n_{\mathrm{eff}}), L_{\mathrm{spp}}, A_{\mathrm{n}}$ and FOM in terms of wavelength, which are plotted for $a = 50$ nm, $b = 4a, t_{\mathrm{Ge}} = 0$ and different values of $t_{\mathrm{Mg}\;2}$. So that $t_{\mathrm{Mg}\;2} =$ $10, 15, 20$ nm. As can be seen in Fig. 5(a), the value of $\mathrm{Re}(n_{\mathrm{eff}})$ for a certain $t_{\mathrm{MgF_2}}$ decreases with the increase of the wavelength. In addition, this value for a certain a wavelength decreases with the increase of the dielectric thickness. Figure 5(b) shows that the propagation length L_{spp} increases with the increase of the wavelength and decreases with the increase of the thickness of $\mathrm{MgF_2}$ dielectric layer. It can be seen in Fig. 5(c) that A_{n} for a specific dielectric thickness decreases slightly with the increase of the wavelength and is of the order of 10^{-2}, but for a certain wavelength, the process of A_{n} changes is different from the dielectric layer thickness.

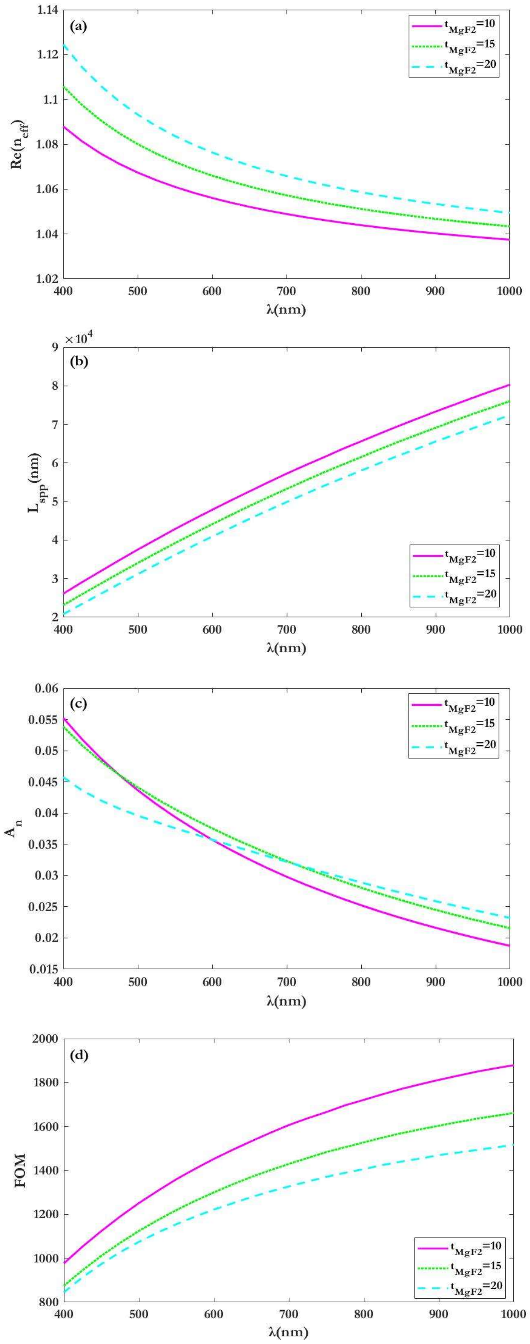

Figure 5. Properties of nano-waveguide with constant consideration of semi-major axis *b=4a* and different values of $t_{\mathrm{MgF_2}}$. (a) $\mathrm{Re}(n_{\mathrm{eff}})$,(b) L_{spp},(c) A_{n} and (d) FOM.

Finally, in Fig. 5(d) the graph of the dependence of the figure of merit FOM on the wavelength is drawn, which is similar to Fig. 5(b), the value of this quantity increases with the increase of the wavelength and decreases with the increase of the thickness of the dielectric layer.

Figure 6 shows the dependence of $\mathrm{Re}(n_{\mathrm{eff}}), L_{\mathrm{spp}}, A_{\mathrm{n}}$ and FOM on the thickness of the second dielectric layer of germanium with size $t_{\mathrm{Ge}} = 5$ nm, for different values of the semi-major axis of the elliptical cylinder nickel nanowire with sizes $b = 50, 100, 200$ nm.

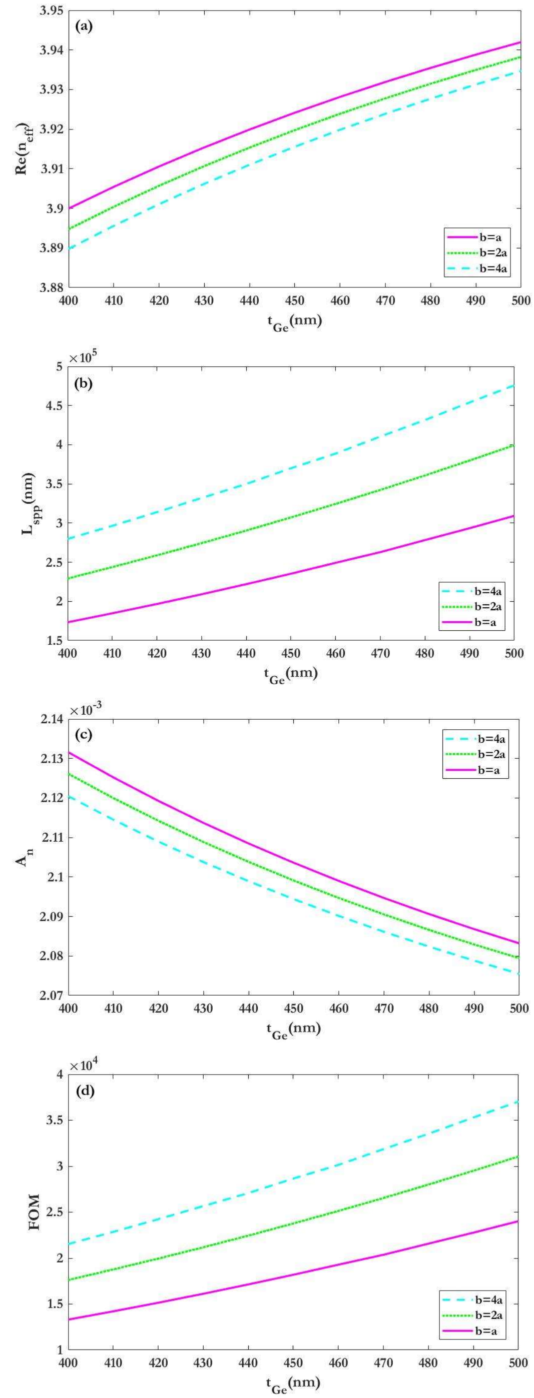

Figure 6. Dependence of nano-wave properties on $t_{\mathrm{Ge}} = 5$ nm.(a) $\mathrm{Re}(n_{\mathrm{eff}})$,(b) L_{spp},(c) A_{n} and (d) FOM.

It can be seen in Fig. 6(a) that the size of $\mathrm{Re}(n_{\mathrm{eff}})$ increases with the increase of the thickness of the dielectric layer t_{Ge} and for a certain value of the thickness of the dielectric layer t_{Ge}, the size of $\mathrm{Re}(n_{\mathrm{eff}})$

decreases with the increase of the semi-major axis. In Figs. 6(b) and 6(d), it can be seen that the propagation length L_{spp} and the figure of merit FOM increase with the increase of the thickness of the dielectric layer t_{Ge}, and for a certain value of the thickness of the dielectric layer t_{Ge}, its size decreases with the increase of the semi-major axis of the nanowire cross-section. Finally, in Fig. 6(c), the dependence of A_{n} on the thickness of the dielectric layer t_{Ge} can be seen, its size decreases with the increase in the thickness of the dielectric layer, and for a value of the thickness of the dielectric layer, the value of A_{n} decreases with the increase of the semi-major axis of the nanowire cross-section. Hence, the proposed waveguide shows longer propagation length and better figure of merit than the similar plasmonic waveguides (e.g., see [40, 41]).

3 Conclusions

In this article, a cylinder elliptical plasmonic nanowaveguide based on nickel metal was investigated in NIR range. The results of the investigation of this nanowaveguide show that in the case where $b=4a$,$t = th = 0$ nm, in the range of $\lambda = 400 - 1000$ nm, the propagation length $L_{\mathrm{spp}} = 99.92726$ nm and the figure of merit $FOM = 84.2883$ and the lowest value for the normalized mode area $A_{\mathrm{n}} = 0.00912$ is obtained. In the condition that $b=4a$ and the thickness of the first dielectric layer, we considered the values of $t_{\mathrm{MgF_2}} = 10, 15, 20$ nm, when $t_{\mathrm{MgF_2}} = 10$ nm, the propagation length $L_{\mathrm{spp}} = 21.81906$ nm and $FOM = 75.1905$ and $A_{\mathrm{n}} = 0.017$, which had significant and better results than the other two modes. Finally, when we considered two layers of dielectric coating with thicknesses of $t_{\mathrm{Ge}} = 400$ nm and $t_{\mathrm{MgF_2}} = 5$ nm for the plasmonic nanowaveguide, the best case and results were obtained for $b=a$, so that L_{spp}=63.481668 nm and $FOM = 22.37486$ and $A_{\mathrm{n}} = 0.002$. The obtained results indicate that the ellipsoidal cylinder plasmonic waveguide based on nickel metal has not only lower losses, but also a measure of competence and longer propagation length and a stronger field enclosure than sodium. It shows that it can be used in high-performance infrared plasmonic devices.

References

[1] A. Asadi, M. R. Jafari, and M. Shahmansouri, “Characteristics of a Symmetric Mid-infrared Graphene Dielectric Hybrid Plasmonic Waveguide with Ultra-deep Subwavelength Confinement.” Plasmonics, **17** (2022) 1819.

[2] M. R. Jafari, and A. Asadi, “Modeling a high-performance broadband mid-infrared modulator using graphene-based hybrid plasmonic waveguide.” Journal of interfaces thin films and low dimensional systems, **5** (2022) 505.

[3] M. R. Jafari, and M. Omidi, “The effect of quantum ring size on shifting the absorption coefficient from infrared region to ultraviolet region.” Applied Physics A, **125** (2019) 1.

[4] M. R. Jafari, F. Ebrahimi, and M. Nooshirvani, “Subwavelenght electromagnetic energy transport by stack of metallic nanorings.” Journal of Applied Physics, **108** (2010) 054313.

[5] K. Zheng, J. Song, and J. Qu, “Hybrid low-permittivity slot-rib plasmonic waveguide based on monolayer two-dimensional transition metal dichalcogenide with ultra-high energy confinement.” Optics Express, **26** (2018) 15819.

[6] B. Pierre, “Long-range surface plasmon polaritons.” Advances in Optics and Photonics, **1** (2009) 484.

[7] V. G. Achanta, “Surface waves at metal-dielectric interfaces: Material science perspective.” Reviews in Physics, **5** (2020) 100041.

[8] M. I. Stockman, “Nanofocusing of optical energy in tapered plasmonic waveguides.” Physical Review Letters, **93** (2004) 137404.

[9] H. Wei, D. Pan, S. Zhang, Z. Li, Q. Li, N. Liu, W. Wang, and H. Xu, “Plasmon waveguiding in nanowires.” Chemical Reviews, **118** (2018) 2882.

[10] J. W. Liaw, S. Y. Moa, J. Y. Luo, Y. C. Ku, and M. K. Kuo, “Surface plasmon polaritons of higher-order mode and standing waves in metallic nanowires.” Optica Express, **29** (2021) 18876.

[11] D. Teng, Q. Cao, S. Li, and H. Gao, “Tapered dual elliptical plasmon waveguides as highly efficient terahertz connectors between approximate plate waveguides and two-wire waveguides.” Journal of the Optical Society of America A, **31** (2014) 268.

[12] D. Liu, S. Zhao, B. You, S. Jhuo, J. Lu, S. Chou, and T. Hattori, “Tuning transmission properties of 3D printad metal rod arrays by breaking the structural symmetry.” Optics Express, **29** (2021) 538.

[13] M. R. Jafari, and F. Ebrahimi, “Plasmonic Thermal Conductance of stack of Metallic Nanorings.” Journal of Sciences Islamic Republic of Iran, **21** (2010) 279.

[14] E. Moreno, SG. Rodrigo, SI. Bozhevolnyi, L. Martín-Moreno, FJ. García-Vidal, “Guiding and Focusing of Electromagnetic Fields with Wedge Plasmon Polaritons.” Physical Review Letters, **100** (2008) 023901.

[15] Z. Han, IP. Radko, N. Mazurski, B. Desiatov, J. Beermann, O. Albrektsen, U. Levy, and SI. Bozhevolnyi, “On-chip detection of radiation guided by dielectric-loaded plasmonic waveguides.” Nano Letters, **15**, (2015) 476.

[16] M. Shahmansouri. B. Farokhi, and R. Aboltaman, “Exchange interaction effects on low frequency surface waves in a quantum plasma slab.” Physics of Plasmas, **24** (2017) 054505.

[17] M. Shahmansouri, and M. Mahmodi-Moghadam, “Quantum electrostatic surface waves in a hybrid plasma waveguide, Effect of nano-sized slab.” Physica of Plasmas, **24** (2017) 102107.

[18] M. Mahmodi-Moghadam, M. Shahmansouri. and B. Farokhi, “Propagational characteristics in a warm hybrid plasmonic waveguide.” Physics of Plasmas, **24** (2017) 122102.

[19] R. F. Oulton, V. J. Sorger, D. A. Genov, D. F. P. Pile, and X. Zhang, A hybrid plasmonic waveguide for subwavelength confinement and long-range propagation. Nature Photonics, **2** (2008) 496.

[20] Y. Ma, J. Li, M. Cada, Y. Bian, Z. Han, Y. Ma, M. Iqbal, and J. Pištora, “Plasmon Generation and Routing in Nanowire-Based Hybrid Plasmonic Coupling Systems With Incorporated Nanodisk Antennas.” IEEE Journal of Selected Topics in Quantum Electronics, **27** (2021) 1.

[21] L. Chen, T. Zhang, X. Li, and W. Huang, “Navel hybrid plasmonic waveguide consisting of two identical dielectric nanowires symmetrically placed on each side of a thin metal film.” Optics Express, **20** (2012) 20535.

[22] D. Teng, Y. Wang, T. Xu, H. Wang, Q. Shao, and Y. Tang, “Symmetric graphene dielectric nanowaveguides as ultra-compact photonic structures.” Nanomaterials, **11** (2021) 1281.

[23] D. Teng, Q. Cao, H. Gao, K. Wang, and M. Zhu, “Three-wave approximation for the modal field inside high-index dielectric rods of hybrid plasmonic waveguides.” Journal of Modern Optics, **63** (2016) 1451.

[24] M. Z. Alam, J. S. Aitchison, and M. Mojahedi, “A marriage of convenience: Hybridization of surface plasmon and dielectric waveguide modes.” Laser & Photonics Reviews, **8** (2014) 1863.

[25] Y. Bian, Z. Zhang, X. Zhao, J. Zhu, and T. Zhou, “Symmetric hybrid surface plasmon polariton waveguides for 3D photonic integration.” Optics Express, **17** (2009) 21320.

[26] D. Dai, and S. He, “A silicon-based hybrid plasmonic waveguide with a metal cap for a nano-scale light confinement.” Optics Express, **17** (2009) 16646.

[27] S. Kumar, P. Kumar, and R. Ranjan, “A metal-cap wedge shape hybrid plasmonic waveguide for nano-scale light confinement and long propagation range.” Plasmonics, **17** (2022) 95.

[28] Q. Zhang, J. Pan, S. Wang, Y. Du, and J. Wu, “A triangle hybrid plasmonic waveguide with long propagation length for ultradeep subwavelength confinement.” Crystals, **12** (2022) 64.

[29] C. C. Huang, R. J. Chang, and C. C. Huang, “Nanostructured hybrid plasmonic waveguide in a slot structure for high-performance light transmission.” Optics express, **29** (2021) 29341.

[30] P. Sun, P. Xu, Z. Zhu, and Z. Zhou, "Silicon-based optoelrctronics enhanced by hybrid plasmon polaritons: Bridging dielectric photonics and nanoplasmonics." Photonics, **8** 482 (2021).

[31] M. Sun, J. Tian, and L. Li, "Mode properties of a coaxial multi-layer hybrid surface plasmon waveguide." Physica Status Solidi b, **252** (2015) 1884.

[32] D. Teng, Q. Cao, and K. Wang, "An extension of the generalized nonlocal theory for the mode analysis of plasmonic materials." Laser & Photonics Reviews, **4** (2017) 795.

[33] K. Zheng, J. Song, and J. Qu, "Hybrid low-permittivity slot-rib plasmonic waveguide based on monolayer two-dimensional transition metal dichalcogenide with ultra-high energy confinement." Optics Express, **26** (2018) 15819.

[34] J. Zhang, Q. Hong, J. Zou, Q. Meng, S. Qin, and Z. Zhu, "Ultra-narrowband visible light absorption in a monolayer MoS_2 based resonant nanostructure." Optics Express, **28** (2020) 27608.

[35] J. Sun, Y. Li, H. Hu, W. Chen, D. Zeng, S. Zhang, and H. Xu, "Strong plasmon-exciton coupling in transition metal dichalcogenides and plasmonic nanostructures." Nanoscale, **13** (2021) 4408.

[36] Y. Wang, J. Yu, Y. F. Mao, J. Chen, and J. Zhu, "Stable, high-performance sodium-based plasmonic devices in the near infrared." Nature, **581** (2020) 401.

[37] J. Gao, C. Hou, F. Wang, H. Liu, and T. Ma, "A directional coupler based on graphene-enhanced Na-loaded plasmonic rib waveguide." Optics Communications, **499** (2021) 127316.

[38] T. Ma, J. Ma, H. Liu, Y. Tian, S. Liu, and F. Wang, "Electro-optic tunable directional coupler based on a LiNbO_3/Na surface plasmonic waveguide." Acta Physica Sinica, **71** (2022) 054205.

[39] A. Asadi, M. R. Jafari, and M. Shahmansouri, "Simulation optimized design of graphene-based hybrid plasmonic waveguide." Indian Journal of Physics, **97** (2023) 2515.

[40] M. R Jafari, A. Asadi, M. Shahmansouri. "Ultra-deep Subwavelength Confinement Palladium-Based Elliptical Cylinder Plasmonic Waveguide in the Near-Infrared range." Plasmonics, **18** (2023) 1037.

[41] D. Teng, Y. Tian, X. Hu, Z. Guan, W. Gao, P. Li, H. Fang, J. Yan, and K. Wang, "Sodium-Based CYLINDRICAL Plasmonic Waveguides in the Near-Infrared." Nanomaterials, **12** (2022) 1950.

[42] E. Silaeva, L. Saddier, and J. P. Colombier, "Drude-Lorentz Model for Optical Properties of Photoexcited Transition Metals under Electron-Phonon Nonequilibrium." Applied Sciences, **11** (2021) 9902.

[43] M. R. Jafari, A. Asadi, and M. Shahmansouri, "Design of Graphene Hybrid Dielectric Plasmonic Nano-waveguide with Ultralow Propagation Loss." Journal of Electronic Materials, **52** (2023) 6483.